

# Dalton Transactions

An international journal of inorganic chemistry

www.rsc.org/dalton

Volume 42 | Number 24 | 28 June 2013 | Pages 8521–8962



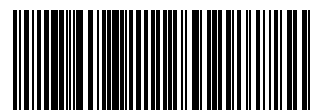
ISSN 1477-9226

RSC Publishing

**COVER ARTICLE**

Petzold *et al.*

Biphenyl bridged hexadentate N<sub>6</sub>-ligands – a rigid ligand backbone for Fe(II) spin crossover complexes



1477-9226 (2013) 42:24;1-M

## Biphenyl bridged hexadentate N6-ligands – a rigid ligand backbone for Fe(II) spin crossover complexes†

Cite this: *Dalton Trans.*, 2013, **42**, 8575

Silvio Heider,<sup>a</sup> Holm Petzold,<sup>\*a</sup> Guillaume Chastanet,<sup>b</sup> Stephan Schlamp,<sup>c</sup> Tobias Rüffer,<sup>a</sup> Birgit Weber<sup>c</sup> and Jean-François Létard<sup>b</sup>

The novel hexadentate nitrogen based ligand *N,N'*-bis-(2-(1*H*-pyrazol-1-yl)pyridine-6-ylmethyl)-2,2'-biphenylenediamine (**3**) was synthesized and used for the preparation of iron Spin Crossover (SCO) complexes [Fe(**3**)](BF<sub>4</sub>)<sub>2</sub> (**4**) and [Fe(**3**)](ClO<sub>4</sub>)<sub>2</sub> (**5**), which differ only by the respective counter ion. These complex salts show different spin transition temperatures  $T_{1/2}$  (135 and 157 K, respectively). This effect was studied by the investigation of the solid state structure of different low- and high-spin isomers. All complexes of this series show closely related crystal packing regardless of the counter ion, metal (Zn/Fe) and spin state. The isomer exhibiting the lower transition temperature (**4**) was also investigated in respect to its photomagnetic behaviour. The LIESST process could be monitored for this complex, but no reverse-LIESST was observed. The relaxation of the photo-induced state occurs at ca. 80 K, showing a complex, three-state relaxation mechanism.

Received 15th October 2012,  
Accepted 30th November 2012

DOI: 10.1039/c2dt32451b

www.rsc.org/dalton

### Introduction

Spin Crossover (SCO) complexes have gained a huge interest, as they can change their spin state by external perturbation, *e.g.* change of temperature or pressure, light irradiation or guest molecules.<sup>1–8</sup> The associated changes of color, magnetism, refractive index, *etc.* are promising for applications like displays, data storage or sensors.<sup>2,9–11</sup> SCO complexes must contain a metal ion able to be present in its low-spin (LS) and its high-spin (HS) states. This is particularly the case for Fe(II) which in a suitable octahedral ligand field exhibits a diamagnetic (LS,  $S = 0$ )  $\leftrightarrow$  paramagnetic (HS,  $S = 2$ ) crossover. The most appropriate ligand field is given by N6 coordination spheres leading to a suitable orbital splitting  $\Delta_o$  (10 Dq) for

the observation of an equilibrium between the HS and LS states.<sup>3,5,12–19</sup> In the high-spin form the anti-bonding  $e_g$  orbitals are filled with two electrons, while in the case of the low-spin form only the non-bonding  $t_{2g}$  orbitals are filled. Thus huge structural changes are observed along the SCO due to Fe–N bond length variations around 0.2 Å.<sup>20</sup> Furthermore the high-spin isomers often expose large deviations from the octahedral geometry, while the corresponding low-spin isomers show less distorted  $O_h$  coordination spheres.<sup>18,20–24</sup>

It has been shown that those great structural changes associated with a rigid ligand scaffold increase the lifetime of the photo-induced state reached by the LIESST phenomenon.<sup>6,19,25–27</sup> This might be due to an increased activation energy for rotational vibration modes, as shown by Hendrickson *et al.*<sup>28</sup> This is particularly visible on the evolution of  $T(\text{LIESST})$ , the temperature above which the photo-induced state is erased, upon ligand denticity and rigidity.<sup>6,26</sup> Therefore we are interested in covalently fixed hexadentate nitrogen ligands which are able to coordinate in an octahedral fashion, the covalent linking of nitrogen donors should lead to increasing distortions upon SCO. Only a few examples have been investigated in detail.<sup>29–35</sup>

Recently, we reported a facile synthesis of such ligands and of the obtained Fe(II) SCO complexes **7–9**,<sup>36</sup> which showed an interdependency of the SCO transition temperature and the substitution pattern in the backbone due to sterical effects. Herein we want to report the electronic and structural modification of those complexes by replacing a pyridyl moiety with a 1*H*-pyrazol-1-yl fragment and the investigations of the resulting iron(II) SCO (**4/5**) complexes (Fig. 1).

<sup>a</sup>Fakultät für Naturwissenschaften, Institut für Chemie, Lehrstuhl für Anorganische Chemie, Technische Universität Chemnitz, Straße der Nationen 62, 09111 Chemnitz, Germany. E-mail: holm.petzold@chemie.tu-chemnitz.de;

Fax: +49 (0)371 531-837463; Tel: +49 (0)371 531-37463

<sup>b</sup>ICMBC – CNRS (UPR 9048), Université Bordeaux I, 87 Av. du Doc. A. Schweitzer, 33608 Pessac, France. E-mail: letard@icmcb-bordeaux.cnrs.fr;

Fax: +33 (0)540 00 26 49; Tel: +33 (0)540 00 83 23

<sup>c</sup>Anorganische Chemie II, Universität Bayreuth, Universitätsstraße 30, 95440 Bayreuth, Germany. E-mail: weber@uni-bayreuth.de; Fax: +49-(0)921/55-2157; Tel: +49-(0)921/55-2555

†Electronic supplementary information (ESI) available: The experimental data for zinc complex **8**, pictures of NMR spectra, the crystallographic data and representations of the complex structures of **4**, **5** and **6**, the relaxation kinetics for the LIESST measurements as well as the details for the XRPD experiments on **4** are available. CCDC 895358, 895359, 895360, 895361, 895362, 895363. For ESI and crystallographic data in CIF or other electronic format see DOI: 10.1039/c2dt32451b

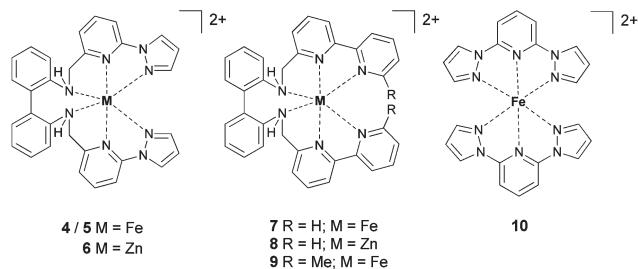


**Fig. 1** Structure of novel complexes **4–6** and comparison with recently published systems **7–9** and related bpp-complexes.<sup>37</sup>

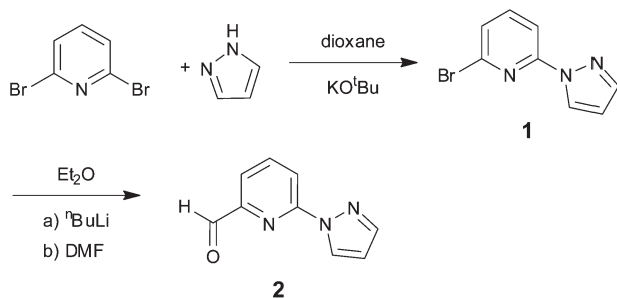
## Results and discussion

### Synthesis

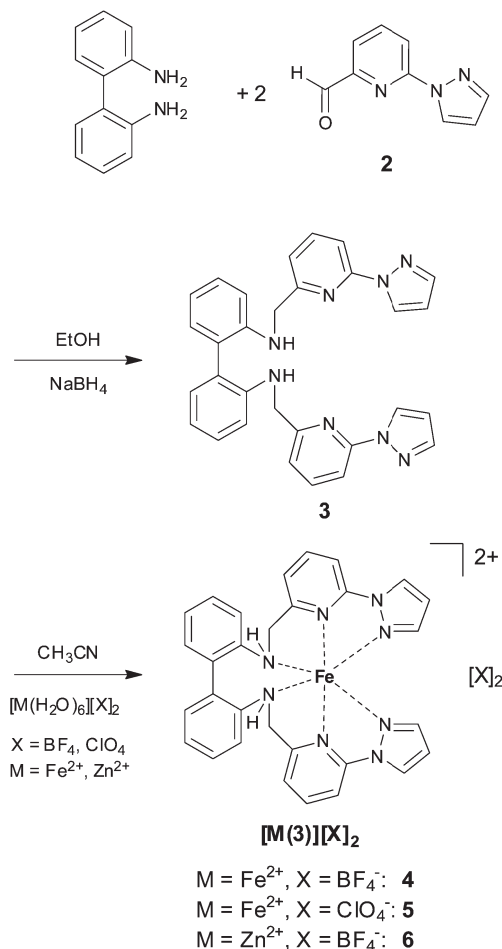
First of all 2-(1*H*-pyrazol-1-yl)pyridine-6-carbaldehyde<sup>38</sup> was synthesized by an improved methodology compared to the existing ones<sup>38,39</sup> (see the Experimental section). In this two-step process first 2,6-dibromopyridine and 1*H*-pyrazole give a mixture of di- and mono-substitution products, *i.e.* 2,6-di(1*H*-pyrazol-1-yl)pyridine and 2-bromo-6-(1*H*-pyrazol-1-yl)pyridine. Inspired by the previously published procedure for the synthesis of substituted bipyridines by Negishi cross coupling and the easily attempted purification of the appropriate low-soluble zinc complex,<sup>36</sup> we tried a similar purification method for this reaction mixture.

Indeed successive addition of ZnCl<sub>2</sub>(*x*H<sub>2</sub>O) to the mixture of 2,6-di(1*H*-pyrazol-1-yl)pyridine and 2-bromo-6-(1*H*-pyrazol-1-yl)pyridine precipitates first the 2,6-di(1*H*-pyrazol-1-yl)pyridine complex and upon further addition of ZnCl<sub>2</sub>(*x*H<sub>2</sub>O) the desired 2-bromo-6-(1*H*-pyrazol-1-yl)pyridine complex. This selective formation allows the easy separation of both compounds by filtration or centrifugation. Adequate workup by treatment of the zinc complex with ammonium hydroxide or EDTA solution leads to the desired compound **1** in 60% yield, with high purity and without any use of column chromatography.<sup>40,41</sup> Therefore we assume that this method is less time and solvent consuming.

A reaction of bromopyridine **1** in diethyl ether at *ca.* –80 °C with one equiv. of <sup>*n*</sup>BuLi followed by the addition of *N,N*-dimethylformamide (DMF) gave 2-(1*H*-pyrazol-1-yl)pyridine-6-carbaldehyde (**2**) quantitatively as a pale-yellow solid (Scheme 1).



**Scheme 1** Synthesis of aldehyde **2**.



**Scheme 2** Synthesis of ligand **3** and the corresponding complexes **4–6**.

The synthesis of compound **3** was accomplished in an analogous manner as previously described.<sup>36</sup> Biphenylene-2,2'-diamine was converted with 2 equiv. of aldehyde **2** in EtOH to the corresponding Schiff base and then reduced *in situ* with NaBH<sub>4</sub> to give the secondary amine **3** in good yields and high purity (Experimental section). Subsequently, diamine **3** was reacted with 1 equiv. of [Fe(H<sub>2</sub>O)<sub>6</sub>][BF<sub>4</sub>]<sub>2</sub>, [Fe(H<sub>2</sub>O)<sub>6</sub>][ClO<sub>4</sub>]<sub>2</sub> or [Zn(H<sub>2</sub>O)<sub>6</sub>][BF<sub>4</sub>]<sub>2</sub> to give complexes [Fe(3)][BF<sub>4</sub>]<sub>2</sub> (**4**), [Fe(3)][ClO<sub>4</sub>]<sub>2</sub> (**5**) and [Zn(3)][BF<sub>4</sub>]<sub>2</sub> (**6**), respectively, which were precipitated by addition of diethyl ether and thereafter yielded purely (Scheme 2).

### Physical measurements

**NMR spectroscopy.** The <sup>1</sup>H NMR spectra of diamine **3** show the expected signals, *i.e.* the signals for the CH<sub>2</sub> and NH protons at 4.40 and 5.13 ppm, respectively, and in the range from 6.3–8.0 ppm the signals of the aromatic bonded protons appear. The same expected behaviour is found for the <sup>13</sup>C{<sup>1</sup>H} NMR, where one signal at 48.1 ppm represents the methylene group, whereas 14 signals in the region from 107–157 ppm match the structure of the aromatic part. In the case of the iron complexes **4** and **5** thirteen signals can be found in the <sup>1</sup>H NMR spectrum (Fig. 2), the CH<sub>2</sub> protons are diastereotopic

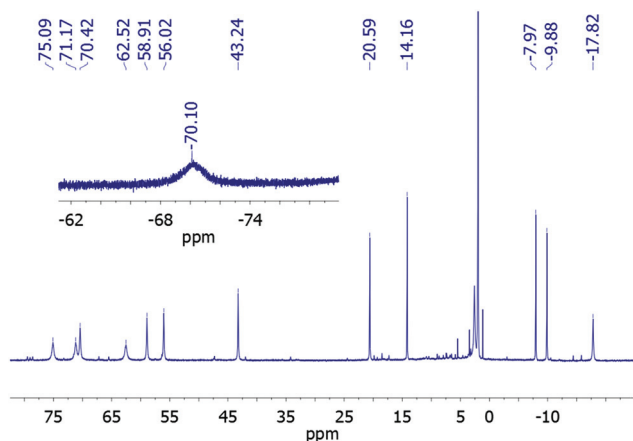


Fig. 2  $^1\text{H}$  NMR spectrum of complex  $[\text{Fe}(3)](\text{ClO}_4)_2$  (**5**) in  $\text{CD}_3\text{CN}$  at 298 K.

due to the fixed arrangement of the biphenyl connectivity upon complexation. Also these signals are spread from *ca.* -70 to 75 ppm, which is common for paramagnetic complexes.<sup>1,36,42,43</sup>

Additionally, other small signals appear, which seem to belong to another paramagnetic complex. As the elemental analyses and mass spectra fit well to the desired complexes, this paramagnetic complex probably is another stereoisomer, because NMR spectra in  $d_6$ -acetonitrile also show those signals, although the solubility of the complex is low (ESI, Fig. S4†). However partial hydrolysis cannot be ruled out as origin of those signals. The analogous zinc complex **6** also shows 10 signals for the aromatic protons, two for the diastereotopic  $\text{CH}_2$  protons and one for the NH protons, respectively (see the Experimental section/ESI Fig. S5†).

Thus the complex  $[\text{Fe}(3)]^{2+}$  is present in its high-spin configuration at room temperature, in contrast to the previously published complex **7**, where the pyrazolyl fragment is substituted by a pyridine moiety (Fig. 1) and shows almost 100% low-spin character at room temperature.<sup>36</sup> This is on the one hand attributable to the lower  $\sigma$ -donor- and  $\pi$ -acceptor-capabilities of pyrazol compared with pyridine;<sup>32,44</sup> on the other hand in this ligand system the incorporation of the pyrazolyl moiety also leads to less favourable bond angles (*vide infra*). Nevertheless, the splitting of the  $\text{CH}_2$  signals still indicates the  $C_2$  symmetry and therefore proves the stability of the complexes with regard to ligand exchange and solvolysis in acetonitrile.

### Magnetic properties

The magnetic behaviour of complex **4** was investigated in solution by Evans' method<sup>45</sup> in  $\text{CD}_3\text{CN}$  and  $(\text{CD}_3)_2\text{CO}$  (Fig. 3). Those data were fitted with the regular solution model (eqn (1)) resulting in  $T_{1/2} = 196$  K,  $\Delta H = 10.8$  kJ mol<sup>-1</sup> and  $\Delta S = 55$  J K<sup>-1</sup> mol<sup>-1</sup>.

$$\mu_{\text{eff}} = \frac{5.0\mu_{\text{B}}}{1 + \exp\left(\frac{\Delta H}{R} \left[\frac{1}{T} - \frac{1}{T_{1/2}}\right]\right)} \quad (1)$$

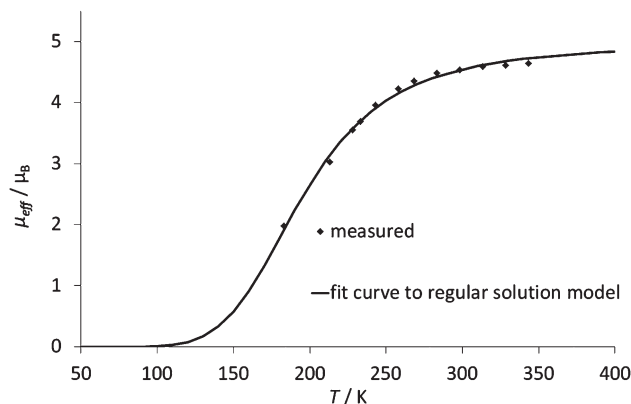


Fig. 3 Fit of the solution susceptibility data to the regular solution model (see information given in the text).

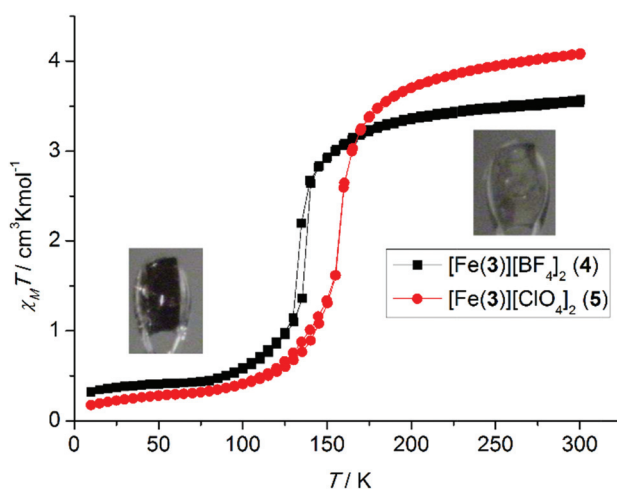
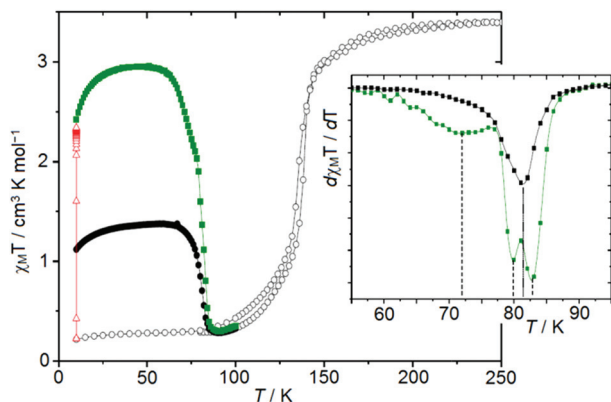


Fig. 4 Magnetic susceptibility data for complexes **4** and **5** in the 10–300 K temperature range with pictures of complex **5** at 298 K (green) and 110 K (violet).

The magnetic behaviour of polycrystalline samples of **4** and **5** were investigated by SQUID measurements from 300 K to 10 K under 0.2 T magnetic field (Fig. 4). At room temperature, the  $\chi_{\text{M}}T$  products ( $\chi_{\text{M}}$  stands for the magnetic molar susceptibility) show typical values for HS Fe(II) complexes with  $\chi_{\text{M}}T = 3.6$ – $4.1$  cm<sup>3</sup> K mol<sup>-1</sup>. Upon cooling, a strong decrease down to  $\chi_{\text{M}}T = 0.2$ – $0.3$  cm<sup>3</sup> K mol<sup>-1</sup> at  $T = 10$  K is observed, typical for LS iron(II) complexes with small paramagnetic residues.<sup>46,47</sup> A spin state crossover can be observed in both salts, one centered at 135 K in **4** (Fig. 3), which shows a narrow hysteresis of approximately 4 K ( $T_{1/2\downarrow} \approx 133$  K,  $T_{1/2\uparrow} \approx 137$  K), the other one centered at 157 K without showing a hysteresis in **5**.

The population of the high-spin metastable state at low temperature was accessible by fast cooling of the sample from room temperature to 10 K. Then, the sample is warmed at the 0.3 K min<sup>-1</sup> scan rate in order to record a  $T(\text{TIESST})$  temperature (TIESST stands for Thermally-Induced Excited Spin-State Trapping).<sup>48,49</sup> Fig. 5 reports this  $T(\text{TIESST})$  curve for compound **4** in comparison with the thermal Spin Crossover



**Fig. 5** LIESST and TIESST measurements for **4**. Open circles: thermal spin transition, black squares: thermally trapped high-spin state, open triangles: photoirradiation at 514 nm, green squares: thermal relaxation of photo-induced high-spin state. The inset in the right shows the first derivative for extraction of  $T(\text{LIESST})$  and  $T(\text{TIESST})$ .

curve. From 10 K to 50 K the small increase of  $\chi_M T$  reflects the presence of zero-field splitting of the paramagnetic HS state. The maximum  $\chi_M T$  value reached at  $\approx 50$  K gives some information on the quench efficiency (40%). Above 50 K the high-spin  $\rightarrow$  low-spin relaxation becomes efficient and the  $\chi_M T$  decreases to recover the low-spin ground state above 80 K. From the derivative of the curve, the  $T(\text{TIESST})$  value of 81 K can be extracted pointing out the position of the minimum (inset in Fig. 5, black curve). This curve will be particularly interesting compared with the one recorded after photo-excitation.

### Photomagnetic properties

The photomagnetic properties of compound **4** have been investigated. The first step was to record the diffuse reflectance thermal behaviour (Fig. 6). At room temperature, the spectrum is mainly constituted by an MLCT band centered at 620 nm with several shoulders at 700 and 750 nm. Around 850 nm a weak band could be observed as a signature of the d-d absorption band of the high-spin isomer. Upon cooling to 100 K the MLCT band increases indicating the population of the low-spin state, in correlation with the decrease of the 850 nm band. The reflectivity signal followed at 620 nm (Fig. 6, inset on the left) indicates a thermal Spin Crossover around 140 K, in good agreement with the magnetic data (*vide supra*). Below 100 K, the reflectivity signal at 620 nm strongly increases in correlation with a decrease of the MLCT absorption band and an increase of the 850 nm band. The spectrum at 10 K is similar to the one at 280 K proving the population of the high-spin state according to the LIESST effect.

Then, susceptibility measurements were carried out on a thin layer of compound **4**. Irradiation was tested at different wavelengths and the best conditions were found to be at 514 nm with a  $1 \text{ mW cm}^{-2}$  power. Whatever the wavelength used (514, 647 and 830 nm), only the LIESST effect was observed and no reverse-LIESST. After the saturation is reached at 10 K, the  $T(\text{LIESST})$  curve was recorded.<sup>50</sup> Almost

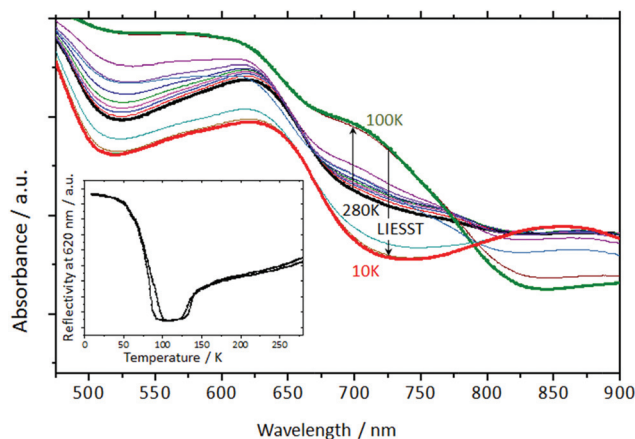


**Fig. 6** Reflectivity measurements on **4** in the range from 280 to 10 K. The inset in the left shows the intensity of the reflectivity at 620 nm over the temperature.

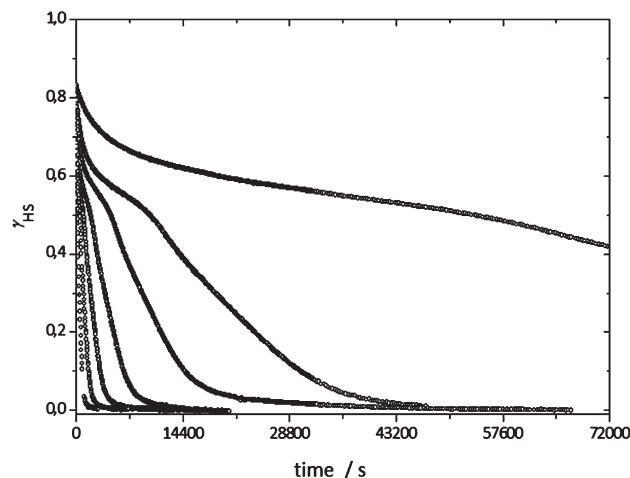


**Fig. 7** Plot of relaxation kinetics of the photo-induced phase (LIESST) in the range from 65 to 82.5 K.

90% of the low-spin molecules are photo-converted into the high-spin metastable phase. The  $T(\text{LIESST})$  curve shape differs from the  $T(\text{TIESST})$  one above 60 K with the occurrence of a two-step transition. The low temperature step appears to be quite gradual, spreading over almost 15 K while the high temperature step presents a sharp transition. The derivative of the  $T(\text{LIESST})$  curve confirms these observations by the presence of two main minima, one very large at 72 K, and one very steep at 82 K (inset in Fig. 5, green curve). A third minimum can even be observed at 80 K which is quite unusual.

Relaxation kinetics have been recorded to characterize the relaxation process of the photo-induced state (Fig. 7). The metastable high-spin state clearly relaxes following a multistep process as a reflect of the  $T(\text{LIESST})$  curve. A first exponential relaxation occurs at short time and two very close relaxations take place at longer delay. At least one of these two last relaxations exhibits a cooperative behavior. The relaxation kinetics of the quickly cooled state have also been investigated (ESI,

Fig. S6†). However those relaxation curves also present two relaxation rates since a first exponential behavior appears at short time and a sigmoidal one at longer times. Therefore, the extraction of the dynamical parameters becomes tricky in both the photo-induced and the quickly-cooled states.

### X-Ray crystallography

The crystal structures of compounds **4** and **5** were investigated by temperature dependent powder and single-crystal X-ray diffraction. The temperature-dependent XRPD measurements for **4** (ESI, Fig. S12–S14†) show first that only one isomorph is present and no other phases with intermediate spin could be observed. Furthermore the same transition temperature as the one extracted from the magnetic characterization was found.

Crystals suitable for X-ray analysis were grown by diffusion of diethyl ether vapors into concentrated solutions of the complex salts **4**, **5**, and **6** in CH<sub>3</sub>CN. The crystallization affords reproducibly well shaped crystals of the complexes without incorporating packing solvents. Data were collected by X-ray diffraction on these crystals at different temperatures and then solved. At all temperatures the lattice of the crystals can be described in monoclinic space groups,  $P2_1/n$  (**4** at 90 K, **5** and **6** at 110 K) and  $P2_1/c$  (**4**, **5** at 295 K).

At low temperature both iron salts as well as the zinc complex **6** show two independent molecules of the complex in the asymmetric unit, while at room temperature for both iron salts only one complex molecule (together with the corresponding anions in all cases) is present. Surprisingly, the corresponding zinc complex **6**, which is a model for an iron(II) high-spin complex, also shows two molecules in the asymmetric unit. This is in contrast to the iron(II) high-spin structures that only show one molecule in the asymmetric unit. The unit cell dimensions of the iron complexes **4** and **5** in the low-spin and high-spin states are closely related as the space groups  $P2_1/n$  and  $P2_1/c$  are interchangeable, moreover the unit cell of the iron complexes **4** and **5** in the high-spin state ( $P2_1/c$ ) can be yielded to a good approximation by simply cutting the unit cell of complex **6** or **4** and **5**, respectively, determined at low temperatures ( $P2_1/n$ ). This is schematically explained in the ESI (Fig. S11†). In contrast to other systems the presence of two different sites for the iron complexes in the crystal lattice

does not lead to a two-step transition, as otherwise often observed.<sup>51–54</sup>

A closer look at the crystal structure revealed only small differences in the atomic distances and angles between the two independent molecules in the low temperature structures; therefore we assume that the phase transition can be explained by the increasing thermal movement of the atoms at room temperature averaging the small structural differences of the independent molecules.

In compound **4** at 90 K Fe–N bond lengths from 1.8945(1)–2.063(2) Å are found, while in **5** the Fe–N bond lengths at 110 K account to 1.911(2)–2.069(3) Å representing a low-spin complex in both cases. At 295 K the Fe–N bond lengths in **4** take values between 2.102(2)–2.238(2) Å and for **5** 2.118(4)–2.252(5) Å, showing a high-spin complex in both cases. This is in agreement with the SCO behavior discussed above.

As mentioned above, the  $T_{1/2}$  value for the SCO in the two iron complexes is different, thus we examined the packing and intra- and intermolecular contacts further, as it is known that hydrogen bonds and  $\pi$ – $\pi$  stacking influence the SCO process and the cooperativity.<sup>10,55</sup> In **4** H–F interactions between the NH groups of the ligand and the BF moieties of the counter ions exist, as well as H–O contacts in **5** between the NH amino groups and the perchlorate counter ions (see ESI, Fig. S10†). As can be seen in Table 1 in the low-spin configurations similar or slightly smaller hydrogen-X (X = O, F) bonds can be found compared to the respective high-spin structures. The differences found are relatively small. The longer contacts found in the high-spin structures in respect to the low-spin isomers may be simply attributed to the higher temperature of data collection, while the differences between BF<sub>4</sub> and ClO<sub>4</sub> salts originate from the different nature of hydrogen interaction to fluorine and oxygen, respectively. This is probably enough to explain the effect of changing  $T_{1/2}$  by about 20 K. For explaining the decreased  $T_{1/2}$  in contrast to the solution, one could assume that the host prefers the high-spin forms as the crystal lattice was originally formed by high-spin complexes at ambient temperature.

Both salts of [Fe(3)]<sup>2+</sup> undergo a spin transition between 90 K and room temperature. This change of the spin state is not only accompanied by the elongation of the bond lengths

**Table 1** Octahedral distortion parameters of complexes **4–10** and short contacts in the solid state structures of complexes **4–6** (see ESI, Fig. S10†)

Complex	$d_{\text{avg}}/\text{\AA}^a$	$\theta/^\circ^b$	$\Delta\theta/^\circ$	$\Sigma/^\circ^c$	$\Delta\Sigma/^\circ$	H-bonds/\AA	$\pi$ – $\pi$ -contacts/\AA
<b>4</b> (ls)	1.97/1.98	256/267	169/180	79.3/80.3	57.5/58.5	2.03–2.35	3.31–3.35
<b>4</b> (hs)	2.17	436		137.8		2.03–2.62	/
<b>5</b> (ls)	1.99/1.98	249/260	175/186	77.2/80	57.4/60.2	2.05–2.13	3.29–3.30
<b>5</b> (hs)	2.18	435		137.4		2.22	/
<b>6</b> (Zn)	2.16	408				2.02–2.50	/
<b>7</b> (ls) <sup>36</sup>	1.97	228		63.6			
<b>8</b> (Zn)	2.16	408	180 <sup>d</sup>				
<b>9</b> (hs) <sup>36</sup>	2.20	420	192 <sup>e</sup>	128.7	65.1 <sup>f</sup>		
<b>10</b> (ls) <sup>19,37</sup>	1.95	282	185	86.1	64.7		
<b>10</b> (hs) <sup>19,37</sup>	2.16	467		150.8			

<sup>a</sup> The average value of the six Fe–N bond lengths. <sup>b</sup> The sum of the deviations from 60° of the hypothetical *fac*-trigonal planes against each other. <sup>c</sup> The sum of the deviations from 90° of the twelve *cis*-angles  $\varphi$  in the octahedral coordination sphere. <sup>d</sup>  $\theta(8) - \theta(7)$ . <sup>e</sup>  $\theta(9) - \theta(7)$ . <sup>f</sup>  $\Sigma(9) - \Sigma(7)$ .

towards higher temperature, but also by a change of the N–Fe–N bond angles. In the low temperature structure those are nearer to an ideal octahedron than in the high-temperature phase. For the distortion in octahedral complexes several parameters were defined,<sup>18,19,28</sup> of which  $\Sigma$  and  $\theta$  shall be introduced and used for these examples.  $\Sigma$  is given by the sum of the deviations of the twelve *cis* N–Fe–N angles  $\varphi$  from 90° (eqn (2)),  $\theta$  is calculated by the sum of the deviations of the N–Fe–N angles  $\theta$  between the projections of the triangular faces from 60° (eqn (3), Fig. 8).

$$\Sigma = \sum_{i=1}^{12} |90^\circ - \varphi_i| \quad (2)$$

$$\theta = \sum_{j=1}^{24} |60^\circ - \theta_j| \quad (3)$$

$\Sigma$  is proportional to the distortion from the octahedral geometry, while  $\theta$  is more indicative of the special distortion towards a trigonal prismatic arrangement and also takes bond length alterations into account. For an ideal octahedron both values are zero, *i.e.*  $\Sigma = \theta = 0$ . For the complex salt **4**  $\Sigma_{\text{ls}} = 79.3^\circ/80.3^\circ$  and for the high-spin complex  $\Sigma_{\text{hs}} = 137.6^\circ$ , while for **5**  $\Sigma_{\text{ls}} = 77.2^\circ/80^\circ$  and  $\Sigma_{\text{hs}} = 137.4^\circ$ . Compared to other complexes, it becomes clear that Fe(II) SCO complexes with bidentate nitrogen donors show much smaller deviations, typically  $\Sigma_{\text{ls}} = 40\text{--}60^\circ$  and  $\Sigma_{\text{hs}} = 70\text{--}85^\circ$ .<sup>19</sup> This demonstrates the fixed structure of the hexadentate ligand system **3**, which cannot adopt an ideal octahedral coordination sphere like it is possible with, for example, three bidentate ligands. Furthermore it can be seen that the difference of the deviation parameters,  $\Delta\Sigma$ , which is approximately 30° for bidentate ligand based complexes,<sup>19</sup> accounts to *ca.* 57–60° for these hexadentate complexes. These values,  $\Sigma_{\text{ls}}$ ,  $\Sigma_{\text{hs}}$  and  $\Delta\Sigma$ , are in quite good accordance with those for  $[\text{Fe}(\text{1-bpp})_2]^{2+}$  (**10**) and a vast amount of similar 2,6-bispyrazolylpyridine iron(II) complexes, where typically  $\Sigma_{\text{hs}}$  lies in the range from 144–158° and  $\Sigma_{\text{ls}}$  lies in the range from 80–96°, resulting in  $\Delta\Sigma$  ranging between 54–70°.<sup>18,19</sup>

Compared to previously reported hexadentate low- and high-spin iron(II) complexes, **7** and **9**, with ligands of similar structures, it can be seen that they show smaller values for  $\Sigma$ , *i.e.*  $\Sigma_{\text{ls}} = 63.6^\circ$  (**7**) and  $\Sigma_{\text{hs}} = 128.7^\circ$  (**9**), showing a less distorted coordination geometry (*vide infra*). The difference between those two complexes, *i.e.*  $\Delta\Sigma = \Sigma(\mathbf{9}) - \Sigma(\mathbf{7}) = 65.1^\circ$ , is even a little larger than for the title compounds **4** and **5**. Hence, it seems clear that the magnitude of structural change upon SCO for this type of iron(II) compound with this 2,2'-diaminobiphenyl N6 ligand system is in every case very large and comparable similar within this series, and also with iron(II) complexes with two tridentate bispyrazolylpyridine ligands on the other hand.

For  $\Delta\theta$  it has been stated that this deviation parameter has much more influence on  $T_{1/2}$  and  $T(\text{LIESST})$  than  $\Delta\Sigma$ .<sup>19</sup> It is obvious that **7** and **9** show a similar, only slightly larger trigonal distortion than **10**, with 192° and 185°, respectively. The respective title compounds **4** and **5** also show similar  $\Delta\theta$

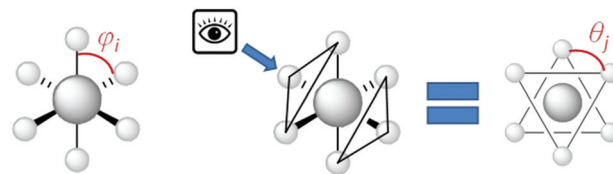


Fig. 8 Definitions of angles  $\varphi_i$  and  $\theta_j$ .

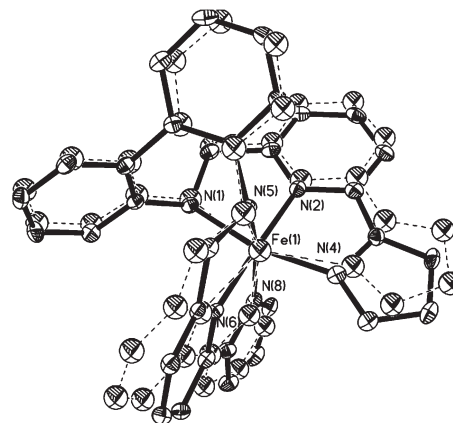


Fig. 9 Overlay of the molecular structure of high-spin (dashed bonds) and low-spin (solid bonds) isomers of complex **5** in the solid state. The atomic positions have been calculated by least square fit using all six ligating nitrogens and the central iron. Thermal ellipsoids were drawn with 35% occupation level.

values, ranging from 169° to 186°. This means that the trigonal distortion upon SCO for **4** and **5** is comparable to that of  $[(1\text{-bpp})_2\text{Fe}][\text{BF}_4]_2$  (**10**).<sup>19</sup> The expectation of a high  $T(\text{LIESST})$  value is not fully met by the found value of  $\approx 80$  K placing complex **4** on the  $T_0 = 120$  K line.<sup>6,26</sup> Interestingly, *tren* ligand based SCO complexes also lie on this  $T_0$  but they undergo a much smaller distortion of the coordination sphere.<sup>33</sup> In contrast, both relaxation kinetics and magnetic measurements showed high cooperative behaviour in the solid state for complexes **4** and **5** reflected by the steep spin transition in both salts and the cooperative relaxation of compound **4** after excitation with light.

In order to find out more about the influence of the ligand on the structural changes we have calculated the elongation of the distances between adjacent nitrogen atoms in the coordination sphere upon SCO. Not surprisingly, these distances change to a greater extent for nitrogen atoms which are not directly connected by the ligand backbone. On average these seven N...N distances differ by 0.41 Å in complex **5**. Much smaller are the changes in the N...N distances within the ligand backbone which are on average 0.12 Å smaller in the low-spin state. Apparently large with 0.25 Å is the difference for the distance N1...N4, the nitrogen atoms bound to the biphenyl bridge, due to the flexibility of the biphenyl moiety. Taking this into account, the average difference within the side arms (N1...N2...N4 and N5...N6...N8) is much smaller with about 0.07 Å. Fig. 9 shows an overlay of the molecular structures of complex **5** in the respective low- and high-spin

states. Due to the fixed ligand backbone the differences between these spin states amplify at the end of the ligand arms, N4 and N8 are replaced by about 0.35 Å from their original positions upon Spin Crossover whereas N1 and N5 are displaced by only 0.2 Å. A rough picture from the molecular structure of the high-spin isomer can be extracted from the zinc complexes **6** and **11**, where bond angles and distortion parameters are almost the same. Using the zinc complex as a model is therefore a good approach to evaluate structural changes in an SCO system if the high-spin structure is not available.

As mentioned above, the bond angles between the metal ion and the terminal pyrazolyl unit are not as ideal as in corresponding pyridine substituted derivatives (**7**, **9**). In all cases, the donating atom is an aromatic nitrogen atom (Fig. 10). As the lone pair is located in an  $sp^2$  orbital in a six membered or five membered aromatic system, the ideal bond angle would be  $120^\circ$  and  $126^\circ$ , respectively. In Table 2 it can be seen that the spin state of the corresponding metal ion in the complex has minor influence on these angles. More important is the geometry of the heterocycle: the six membered terminal pyridine rings in **7** and **9** lead to only small deviations from  $120^\circ$ , moreover the difference between  $\alpha$  and  $\beta$  is small (about  $10^\circ$ ), while the five membered, more strained pyrazole rings in **4** and **5** lead to great deviations from the idealized angle, especially for  $\beta$ , which is in all cases slightly above  $140^\circ$ . Also the difference between  $\alpha$  and  $\beta$  is much larger (about  $30^\circ$ ).

Therefore, the pyrazolyl substituted ligands in **4/5** cannot donate as well to the metal ion as the pyridine substituted derivatives. The lone pair of the pyrazolyl nitrogen points somewhat away from the iron atom. This is one reason for the lower ligand field splitting induced by **3** in comparison to the pyridine derivative. Moreover the higher strain within the

coordinated ligand results in a lower stability of the complexes **4/5** compared to **7/9**.

## Conclusions

We have developed a new, straightforward two-step synthetic route to 2-(1*H*-pyrazol-1-yl)pyridine-6-carbaldehyde (**2**), which was then converted to the novel hexadentate secondary amine **3**, possessing two amino-, two pyridine- and two pyrazolyl-donor functions. With this we synthesized a new Fe(II) SCO complex as two different salts,  $[\text{Fe}(\text{3})][\text{BF}_4]_2$  (**4**) and  $[\text{Fe}(\text{3})][\text{ClO}_4]_2$  (**5**), which show different spin transition temperatures depending on the counter ion, while in solution another different transition temperature is found for  $[\text{Fe}(\text{3})]^{2+}$ . By solution and investigation of the X-ray structures of these salts in their respective low-spin and high-spin forms this effect was attributed to different hydrogen bonding interactions between NH and  $\text{ClO}_4/\text{BF}_4$ , respectively.

Furthermore photomagnetic measurements were carried out on **4**, which showed the lowest transition temperature and thus should feature the highest  $T(\text{LIESST})$ . It was found that the relaxation process for the photo-induced high-spin state is complex and occurs in two or three steps at around 80 K, which places it on the  $T_0 = 120$  K line of the  $T(\text{LIESST})$  vs.  $T_{1/2}$  database proposed by Létard *et al.*<sup>6,26</sup>

Currently we are working on further studies to vary the ligand and come to an understanding of the LIESST properties of these kinds of complexes.

## Experimental section

### General procedures

All reactions were carried out under an argon inert gas atmosphere using standard Schlenk and cannula techniques. NMR spectra were recorded on a Bruker Avance III 500 spectrometer; chemical shifts for  $^1\text{H}$  and  $^{13}\text{C}$  are referenced internally to the residual protons and to the  $^{13}\text{C}$ -NMR signal for the deuterated solvent. Elemental analyses were performed using a Thermo FlashAE 1112 analyzer. Mass spectra were recorded on a Bruker micrOTOF-QIIa mass spectrometer operating in ESI mode. Magnetic susceptibility data for **4** and **5** were collected using a Quantum Design MPMS-XL5 SQUID magnetometer under an applied field of 0.2 T over the temperature range 10–300 K in the settle mode at a cooling/warming speed of  $10 \text{ K min}^{-1}$ , measuring the magnetization every 5 K, after the temperature was settled within a 0.5 K accuracy for 10 seconds. All samples were placed in gelatin capsules held within plastic straws. Samples for magnetic and photomagnetic

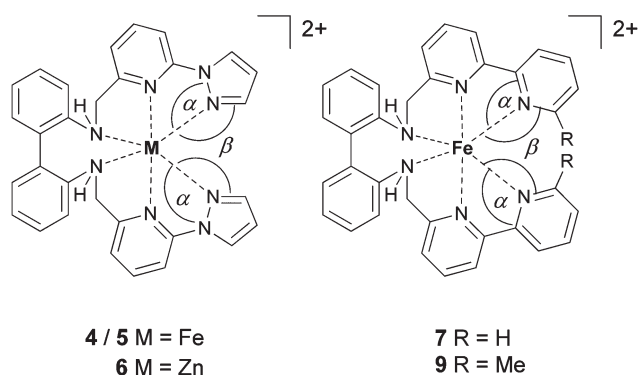


**Fig. 10** Definitions of the angles  $\alpha$  and  $\beta$ , being the bond angles of the terminal nitrogen donor atoms.

**Table 2** Bond angles of the terminal nitrogen donor atom

	<b>4</b> (ls)	<b>4</b> (hs)	<b>5</b> (ls)	<b>5</b> (hs)	<b>6</b> (Zn)	<b>7</b> (ls) <sup>36</sup>	<b>9</b> (hs) <sup>36</sup>
$\alpha/^\circ$	111.4–112.8	113.7–113.9	111.7–111.8	113.1–113.4	111.9–113.5	114.5–114.8	114.3–114.7
$\beta/^\circ$	140.4–142.6	141.4–141.7	141.9–143.0	141.1–141.3	141.0–142.9	126.7–126.8	126.3–126.8

measurements were prepared by crystallization in an analogous manner to the preparation of single crystals. Identity of the structure and that no solvent molecules were incorporated in the lattice was checked by PXRD. The data were corrected for the diamagnetic magnetization of the ligands, which were estimated using tabulated Pascal's constants and of the sample holder. Photomagnetic measurements for **4** were performed using a Spectrum Physics Series 2025 Kr<sup>+</sup> laser (514.5 or 647 nm) or an 830 nm photodiode, coupled by means of an optical fibre to the cavity of an MPMS-5S Quantum Design SQUID magnetometer. The optical power at the sample surface was adjusted to prevent warming of the sample. After being slowly cooled at 10 K the sample in the low-spin state was irradiated and the change in magnetic susceptibility was followed. When the saturation point was reached the laser was switched off and the temperature increased at a rate of  $\approx 0.3$  K min<sup>-1</sup>. The magnetization was measured every 1 K.  $T(\text{LIESST})$  was determined from the minimum of a  $d\chi_M T/dT$  vs.  $T$  plot for the relaxation process. Temperature dependent susceptibility measurements in solution were performed using a Norell NI5CCI-B coaxial insert set. A defined amount of complex was weighted in an NMR tube. This NMR tube was transferred into a Schlenk tube and filled with argon. To this tube a weighted amount of a solution of acenaphthene in d<sub>3</sub>-acetonitrile was added. The tube was sealed with a plastic cap in an argon stream, shaken briefly to dissolve the sample completely and then opened in an argon stream to insert the inset tube, containing the same solution of acenaphthene in d<sub>3</sub>-acetonitrile, into the NMR tube. The determined values were corrected for expansion of the solvent by tabulated values and the effect of deuteration by multiplication with  $M(\text{CD}_3\text{CN})/M(\text{CH}_3\text{CN})$  as described elsewhere.<sup>36</sup>

THF and diethyl ether were purified by distillation from sodium/benzophenone ketyl. Ethanol was purified by distillation from magnesium and acetonitrile by distillation from calcium hydride. Biphenylene-2,2'-diamine<sup>56</sup> was synthesized by following published procedures. All other chemicals were purchased by commercial suppliers and were used without further purification.

**Synthesis of 2-bromo-6-(1H-pyrazol-1-yl)pyridine (1).** This reaction was carried out similarly to the literature procedure.<sup>41</sup> 1H-pyrazol (3.02 g, 44.36 mmol) and 2,6-dibromopyridine (10.51 g, 44.36 mmol) were suspended in 20 mL dry dioxane under an argon atmosphere, KO<sup>t</sup>Bu (4.98 g, 44.36 mmol) was added and the mixture was stirred at 100 °C for 48 h. The solvent was then removed *in vacuo*, water (20 mL) was added and the precipitate was filtrated and washed with water (20 mL). The solid was then dissolved in tetrahydrofuran (20 mL) and ZnCl<sub>2</sub>·nH<sub>2</sub>O (2 g, *ca.* 11.8 mmol) was added which resulted in the precipitation of an off-white solid. This precipitate consists of the zinc chloride complex of the side product 2,6-bis(1H-pyrazol-1-yl)pyridine and of the zinc chloride complex of the desired product. The mixture was then filtrated and the filtrate, which contains the main amount of the desired product and unreacted 2,6-dibromopyridine, was then again treated with ZnCl<sub>2</sub>·nH<sub>2</sub>O (10 g, *ca.* 59 mmol). This

yielded in a further precipitate, which was collected by centrifugation and washed with ether. The precipitate, namely the zinc chloride complex of the desired product, was dissolved in 25% NH<sub>3</sub>(aq.) and CH<sub>2</sub>Cl<sub>2</sub>, the organic phase was separated, the aqueous phase was extracted with CH<sub>2</sub>Cl<sub>2</sub> and the combined organic phases were dried over MgSO<sub>4</sub> and then the solvent was reduced *in vacuo* to yield 2-bromo-6-(1H-pyrazol-1-yl)pyridine (5.97 g, 26.65 mmol, 60%) as a white solid.

<sup>1</sup>H NMR (500 MHz, CDCl<sub>3</sub>):  $\delta$  (ppm) 6.46 (dd,  $J = 2.6, 1.7$  Hz, 1H), 7.34 (dd,  $J = 7.7, 0.6$  Hz, 1H), 7.64 (t,  $J = 7.9$  Hz, 1H), 7.73 (d,  $J = 1.1$  Hz, 1H), 7.92 (dd,  $J = 8.1, 0.6$  Hz, 1H), 8.52 (dd,  $J = 2.6, 0.5$  Hz, 1H).

**Synthesis of 2-(1H-pyrazol-1-yl)pyridine-6-carbaldehyde (2).** 2-Bromo-6-(1H-pyrazol-1-yl)pyridine (1 g, 4.46 mmol) was dissolved in dry diethyl ether (20 mL) under an argon atmosphere, cooled to -80 °C and then <sup>n</sup>BuLi (2.5 M in hexanes, 1.8 mL, 4.5 mmol) was added dropwise. The reaction mixture was stirred at -80 °C for 10 min, whereas the color of the suspension changed from yellow to orange. Then *N,N*-dimethylformamide (DMF, 0.35 mL, 4.5 mmol) was added and the mixture was stirred for a further 10 min while the temperature elevated to -60 °C. To this orange solution hydrochloric acid (37%, 0.5 mL, 6 mmol) was added and the temperature was allowed to rise to room temperature. The reaction mixture was neutralized with NaHCO<sub>3</sub>, H<sub>2</sub>O (25 mL) was added and the product was extracted with diethyl ether (1 × 20 mL) and dichloromethane (1 × 20 mL). The organic phases were collected, dried over MgSO<sub>4</sub> and the volatiles were removed *in vacuo* to give **2** (780 mg, 4.39 mmol, 98.3%) as pale yellow plates.

<sup>1</sup>H NMR (500 MHz, CDCl<sub>3</sub>):  $\delta$  (ppm) 6.48 (dd,  $J = 2.6, 1.7$  Hz, 1H), 7.74 (m, 1H), 7.80 (dd,  $J = 7.5, 0.9$  Hz, 1H), 7.95 (td,  $J = 7.9, 0.8$  Hz, 1H), 8.19 (dd,  $J = 8.2, 0.9$  Hz, 1H), 8.64 (dd,  $J = 2.6, 0.7$  Hz, 1H), 10.01 (d,  $J = 0.7$  Hz, 1H).

**Synthesis of *N,N'*-bis-(2-(1H-pyrazol-1-yl)pyridine-6-ylmethyl)-2,2'-biphenylenediamine (3).** 2,2'-Diamino-1,1'-biphenyl (400 mg, 2.17 mmol) and aldehyde **2** (752 mg, 4.34 mmol) were stirred in dry EtOH (5 mL) under an argon atmosphere for 1 h. The volatiles were then removed *in vacuo*, NaBH<sub>4</sub> (700 mg, 18.5 mmol) and fresh dry EtOH (10 mL) were added and the mixture was refluxed for 2 h. After the mixture had cooled down to room temperature, H<sub>2</sub>O (10 mL) was added and the yellow precipitate was filtrated. This crude product was then recrystallized in EtOH to give the hexadentate amine **3** (560 mg, 1.12 mmol, 51.7%) as pale yellow crystals.

<sup>1</sup>H NMR (500 MHz, CDCl<sub>3</sub>):  $\delta$  (ppm) 4.40 (s, 4H), 5.13 (s, 2H), 6.35 (dd,  $J = 2.4, 1.7$  Hz, 2H), 6.76 (d,  $J = 7.9$  Hz, 2H), 6.88 (td,  $J = 7.4, 0.7$  Hz, 2H), 7.03 (d,  $J = 7.5$  Hz, 2H), 7.23 (dd,  $J = 7.4, 1.5$  Hz, 2H), 7.34 (td,  $J = 8.1, 1.5$  Hz, 2H), 7.50 (t,  $J = 7.8$  Hz, 2H), 7.67 (d,  $J = 1.0$  Hz, 2H), 7.70 (d,  $J = 8.1$  Hz, 2H), 7.98 (d,  $J = 2.4$  Hz, 2H). <sup>13</sup>C{<sup>1</sup>H} NMR (125 MHz, CDCl<sub>3</sub>):  $\delta$  (ppm) 48.12, 107.47, 110.13, 110.97, 117.59, 118.71, 124.41, 127.34, 129.24, 131.08, 138.95, 141.97, 145.46, 150.71, 156.56. ESI-TOF HRMS: 499.2367 (M + H<sup>+</sup>, calc. 499.2353), 521.2173 (M + Na<sup>+</sup>, calc. 521.2173). Anal. calcd (%) for C<sub>30</sub>H<sub>26</sub>N<sub>8</sub>...

3/5EtOH...1/5H<sub>2</sub>O (498.58 g mol<sup>-1</sup>): C 70.73, H 5.71, N 21.15. Found C 70.77, H 5.36, N 20.75.

**Synthesis of [Fe(3)][BF<sub>4</sub>]<sub>2</sub> (4).** The secondary amine 3 (106.5 mg, 0.214 mmol) and [Fe(H<sub>2</sub>O)<sub>6</sub>][BF<sub>4</sub>]<sub>2</sub> (72 mg, 0.214 mmol) were stirred under an argon atmosphere in dry CH<sub>3</sub>CN (5 mL) for 3 h. Then dry Et<sub>2</sub>O (10 mL) was added dropwise to give a greenish precipitate, which was centrifuged and washed with more diethyl ether (5 mL). The green powder was dried *in vacuo* to give complex 4 (120.7 mg, 0.166 mmol, 77.6%).

<sup>1</sup>H NMR (500 MHz, CDCl<sub>3</sub>): δ (ppm) -70.05 (2H), -17.87 (2H), -9.89 (2H), -7.94 (2H), 14.11 (2H), 20.59 (2H), 43.12 (2H), 55.89 (2H), 58.83 (2H), 62.54 (2H), 70.31 (2H), 71.26 (2H), 74.81 (2H). ESI-TOF HRMS: 641.1636 (M-BF<sub>4</sub>, calc. 641.1659); 553.1567 (M-2BF<sub>4</sub>-H, calc. 553.1546); 277.0835 (M-2BF<sub>4</sub>, calc. 277.0810). μ<sub>eff</sub> (25 °C, Evans' method): 4.86 μ<sub>B</sub>. Anal. calcd (%) for C<sub>30</sub>H<sub>26</sub>B<sub>2</sub>F<sub>8</sub>FeN<sub>8</sub> (728.04 g mol<sup>-1</sup>): C 49.49, H 3.60, N 15.39. Found C 48.34, H 3.70, N 15.19.

**Synthesis of [Fe(3)][ClO<sub>4</sub>]<sub>2</sub> (5).** The secondary amine 3 (98.6 mg, 0.198 mmol) and [Fe(H<sub>2</sub>O)<sub>6</sub>][ClO<sub>4</sub>]<sub>2</sub> (71.8 mg, 0.198 mmol) were stirred under an argon atmosphere in 4 mL 1:1 CH<sub>3</sub>CN-CH<sub>2</sub>Cl<sub>2</sub> (v/v) for 3 h. Then dry Et<sub>2</sub>O (10 mL) was added dropwise to give a greenish precipitate, which was centrifuged and washed with more diethyl ether (5 mL). The green powder was dried *in vacuo* to give complex 5 (95.8 mg, 0.127 mmol, 64.3%).

<sup>1</sup>H NMR (500 MHz, CDCl<sub>3</sub>): δ (ppm) -70.05 (2H), -17.87 (2H), -9.89 (2H), -7.94 (2H), 14.11 (2H), 20.59 (2H), 43.12 (2H), 55.89 (2H), 58.83 (2H), 62.54 (2H), 70.31 (2H), 71.26 (2H), 74.81 (2H). μ<sub>eff</sub> (25 °C, Evans' method): 4.92 μ<sub>B</sub>. Anal. calcd (%) for C<sub>30</sub>H<sub>26</sub>Cl<sub>2</sub>FeN<sub>8</sub>O<sub>8</sub> (753.33 g mol<sup>-1</sup>): C 47.83, H 3.48, N 14.87. Found C 47.67, H 3.44, N 14.75.

**Synthesis of [Zn(3)][BF<sub>4</sub>]<sub>2</sub> (6).** The secondary amine 3 (103.4 mg, 0.207 mmol) and [Zn(H<sub>2</sub>O)<sub>6</sub>][BF<sub>4</sub>]<sub>2</sub> (72 mg, 0.207 mmol) were stirred under an argon atmosphere in dry CH<sub>3</sub>CN (5 mL) for 3 h. Then dry Et<sub>2</sub>O (15 mL) was added dropwise to give a pale yellow precipitate, which was centrifuged and washed with more diethyl ether (5 mL). The product was dried *in vacuo* to give complex 6 (135.3 mg, 0.183 mmol, 88.5%).

<sup>1</sup>H NMR (500 MHz, CDCl<sub>3</sub>): δ (ppm) 3.85 (dd, *J* = 18.8, 5.5 Hz, 2H, CH<sub>2</sub>), 4.43 (dd, *J* = 18.8, 9.5 Hz, 2H, CH<sub>2</sub>), 5.31 (dd, *J* = 9.5, 5.5 Hz, 2H, NH), 6.47 (dd, *J* = 8.0, 0.9 Hz, 2H), 6.84 (dd, *J* = 2.8, 2.0 Hz, 2H), 6.92 (td, *J* = 7.8, 1.6 Hz, 2H), 6.97 (dd, *J* = 7.8, 0.5 Hz, 2H), 7.15 (td, *J* = 7.5, 1.1 Hz, 2H), 7.31 (dd, *J* = 7.6, 1.5 Hz, 2H), 7.80 (d, *J* = 1.9 Hz, 2H), 7.9 (m, 2H), 8.10 (t, *J* = 8.0 Hz, 2H), 8.70 (m, 2H). ESI-TOF HRMS: 649.1680 (M-BF<sub>4</sub>, calc. 649.1601), 561.1541 (M-2BF<sub>4</sub>-H, calc. 561.1488), 281.0807 (M-2BF<sub>4</sub>, calc. 281.0780). Anal. calcd (%) for C<sub>30</sub>H<sub>26</sub>B<sub>2</sub>F<sub>8</sub>N<sub>8</sub>Zn (737.57 g mol<sup>-1</sup>): C 48.66, H 3.89, N 14.65. Found C 48.85, H 3.55, N 15.19.

## Acknowledgements

S. H. and H. P. would like to thank the Fonds der Chemischen Industrie for a Liebig-Stipendium and a Doktorandenstipendium.

We also want to thank M. Mehring and M. Schlesinger for the XRPD measurements. S. S. and B. W. thank the University of Bayreuth, the Deutsche Forschungsgemeinschaft (WE 3546\_4-1 and SFB 840/A10) and the Fonds der Chemischen Industrie for financial support. G. C. and J.-F. L. would like to thank the GIS-Advanced Materials in Aquitaine (AMA) and the Aquitaine Region for supporting the development of the ICPA (International Center of Photomagnetism in Aquitaine) platform at the ICMCB.

## Notes and references

- 1 B. Weber, *Coord. Chem. Rev.*, 2009, **253**, 2432–2449.
- 2 O. Sato, J. Tao and Y.-Z. Zhang, *Angew. Chem., Int. Ed.*, 2007, **119**, 2200–2236.
- 3 P. Gütllich and H. A. Goodwin, *Top. Curr. Chem.*, 2004, **233**, 1–47.
- 4 P. Gütllich, A. Hauser and H. Spiering, *Angew. Chem., Int. Ed. Engl.*, 1994, **106**, 2109–2142.
- 5 P. Gütllich, Y. Garcia and H. A. Goodwin, *Chem. Soc. Rev.*, 2000, **29**, 419–427.
- 6 J.-F. Létard, *J. Mater. Chem.*, 2006, **16**, 2550–2559.
- 7 H. Spiering, T. Kohlhaas, H. Romstedt, A. Hauser, C. Bruns-Yilmaz, J. Kusz and P. Gütllich, *Coord. Chem. Rev.*, 1999, **190–192**, 629–647.
- 8 P. J. van Koningsbruggen, Y. Maeda and H. Oshio, *Top. Curr. Chem.*, 2004, **233**, 259–324.
- 9 P. Gamez, J. S. Costa, M. Quesada and G. Aromí, *Dalton Trans.*, 2009, 7845–7853.
- 10 J. A. Real, A. B. Gaspar and M. C. Muñoz, *Dalton Trans.*, 2005, 2062–2079.
- 11 J.-F. Létard, P. Guionneau and L. Goux-Capes, *Top. Curr. Chem.*, 2004, **235**, 221–249.
- 12 J. A. Kitchen and S. Brooker, *Coord. Chem. Rev.*, 2008, **252**, 2072–2092.
- 13 A. Bousseksou, G. Molnár, J. A. Real and K. Tanaka, *Coord. Chem. Rev.*, 2007, **251**, 1822–1833.
- 14 A. Y. Verat, N. Ould-Moussa, E. Jeanneau, B. L. Guennic, A. Bousseksou, S. A. Borshch and G. S. Matouzenko, *Chem.-Eur. J.*, 2009, **15**, 10070–10082.
- 15 J. A. Kitchen, N. G. White, M. Boyd, B. Moubaraki, K. S. Murray, P. D. W. Boyd and S. Brooker, *Inorg. Chem.*, 2009, **48**, 6670–6679.
- 16 M. Haryono, F. W. Heinemann, K. Petukhov, K. Gieb, P. Müller and A. Grohmann, *Eur. J. Inorg. Chem.*, 2009, 2136–2143.
- 17 A. Hauser, *Top. Curr. Chem.*, 2004, **233**, 49–58.
- 18 M. A. Halcrow, *Coord. Chem. Rev.*, 2009, **253**, 2493–2514.
- 19 M. A. Halcrow, *Chem. Soc. Rev.*, 2011, **40**, 4119–4142.
- 20 P. Guionneau, M. Marchivie, G. Bravic, J.-F. Létard and D. Chasseau, *Top. Curr. Chem.*, 2004, **234**, 97–128.
- 21 M. Marchivie, P. Guionneau, J.-F. Létard and D. Chasseau, *Acta Crystallogr., Sect. B: Struct. Sci.*, 2005, **61**, 25–28.
- 22 G. S. Matouzenko, E. Jeanneau, A. Y. Verat and A. Bousseksou, *Dalton Trans.*, 2011, **40**, 9608–9618.

- 23 K. Takahashi, Y. Hasegawa, R. Sakamoto, M. Nishikawa, S. Kume, E. Nishibori and H. Nishihara, *Inorg. Chem.*, 2012, **51**, 5188–5198.
- 24 M. Marchivie, P. Guionneau, J. A. K. Howard, G. Chastanet, J.-F. Létard, A. E. Goeta and D. Chasseau, *J. Am. Chem. Soc.*, 2002, **124**, 194–195.
- 25 J.-F. Létard, L. Capes, G. Chastanet, N. Moliner, S. Létard, J.-A. Real and O. Kahn, *Chem. Phys. Lett.*, 1999, **313**, 115–120.
- 26 J.-F. Létard, P. Guionneau, O. Nguyen, J. S. Costa, S. Marcén, G. Chastanet, M. Marchivie and L. Goux-Capes, *Chem.–Eur. J.*, 2005, **11**, 4582–4589.
- 27 C. Carbonera, J. S. Costa, V. A. Money, J. Elhaik, J. A. K. Howard, M. A. Halcrow and J.-F. Létard, *Dalton Trans.*, 2006, 3058–3066.
- 28 J. K. McCusker, A. L. Rheingold and D. N. Hendrickson, *Inorg. Chem.*, 1996, **35**, 2100–2112.
- 29 L. J. Wilson, D. Georges and M. A. Hoselton, *Inorg. Chem.*, 1975, **14**, 2968–2975.
- 30 L. L. Martin, K. S. Hagen, A. Hauser, R. L. Martin and A. M. Sargeson, *J. Chem. Soc., Dalton Trans.*, 1988, 1313–1315.
- 31 M. Koikawa, K. B. Jensen, H. Matsushima, T. Tokii and H. Toftlund, *J. Chem. Soc., Dalton Trans.*, 1998, 1085–1086.
- 32 H. Toftlund and J. J. McGarvey, *Top. Curr. Chem.*, 2004, **233**, 151–166.
- 33 H. Z. Lazar, T. Forestier, S. A. Barrett, C. A. Kilner, J.-F. Létard and M. A. Halcrow, *Dalton Trans.*, 2007, 4276–4285.
- 34 H. Toftlund, *Coord. Chem. Rev.*, 1989, **94**, 67–108.
- 35 A. H. R. Al-Obaidi, K. B. Jensen, J. J. McGarvey, H. Toftlund, B. Jensen, S. E. J. Bell and J. G. Carroll, *Inorg. Chem.*, 1996, **35**, 5055–5060.
- 36 H. Petzold and S. Heider, *Eur. J. Inorg. Chem.*, 2011, 1249–1254.
- 37 J. M. Holland, J. A. McAllister, Z. Lu, C. A. Kilner, M. Thornton-Pett and M. A. Halcrow, *Chem. Commun.*, 2001, 577–578.
- 38 B. Vacher, B. Bonnaud, P. Funes, N. Jubault, W. Koek, M.-B. Assié and C. Cosi, *J. Med. Chem.*, 1998, **41**, 5070–5083.
- 39 F. Zeng and Z. Yu, *Organometallics*, 2009, **28**, 1855–1862.
- 40 D. L. Jameson and K. A. Goldsby, *J. Org. Chem.*, 1990, **55**, 4992–4994.
- 41 X. Sun, Z. Yu, S. Wu and W.-J. Xiao, *Organometallics*, 2005, **24**, 2959–2963.
- 42 G. J. P. Britovsek, J. England and A. J. P. White, *Dalton Trans.*, 2006, 1399–1408.
- 43 C. Vedder, F. Schaper, H.-H. Brintzinger, M. Kettunen, S. Babik and G. Fink, *Eur. J. Inorg. Chem.*, 2005, 1071–1080.
- 44 T. Ayers, S. Scott, J. Goins, N. Caylor, D. Hathcock, S. J. Slattery and D. L. Jameson, *Inorg. Chim. Acta*, 2000, **207**, 7–12.
- 45 D. F. Evans, *J. Chem. Soc.*, 1959, 2003–2005.
- 46 A. Bialonska and R. Bronisz, *Inorg. Chem.*, 2010, **49**, 4534–4542.
- 47 A. Bialonska, R. Bronisz and M. Weselski, *Inorg. Chem.*, 2008, **47**, 4436–4438.
- 48 M. Marchivie, P. Guionneau, J.-F. Létard, D. Chasseau and J. Howard, *J. Phys. Chem. Solids*, 2004, **65**, 17–23.
- 49 N. Paradis, G. Chastanet and J.-F. Létard, *Eur. J. Inorg. Chem.*, 2012, 3618–3624.
- 50 J.-F. Létard, P. Guionneau, L. Rabardel, J. A. K. Howard, A. E. Goeta, D. Chasseau and O. Kahn, *Inorg. Chem.*, 1998, **37**, 4432–4441.
- 51 J. Klingele, D. Kaase, M. H. Klingele, J. Lach and S. Demeshko, *Dalton Trans.*, 2010, **39**, 1689–1691.
- 52 D. Chernyshov, M. Hostettler, K. W. Törnroos and H.-B. Bürgi, *Angew. Chem., Int. Ed.*, 2003, **42**, 3825–3830.
- 53 S. M. Neville, B. A. Leita, G. J. Halder, C. J. Kepert, B. Moubaraki, J.-F. Létard and K. S. Murray, *Chem.–Eur. J.*, 2008, **14**, 10123–10133.
- 54 W. Bauer, W. Scherer, S. Altmannshofer and B. Weber, *Eur. J. Inorg. Chem.*, 2011, 2803–2818.
- 55 B. Weber, W. Bauer, T. Pfaffeneder, M. M. Dîrtu, A. D. Naik, A. Rotaru and Y. Garcia, *Eur. J. Inorg. Chem.*, 2011, 3193–3206.
- 56 R. E. Moore and A. Furst, *J. Org. Chem.*, 1958, **23**, 1504–1506.